

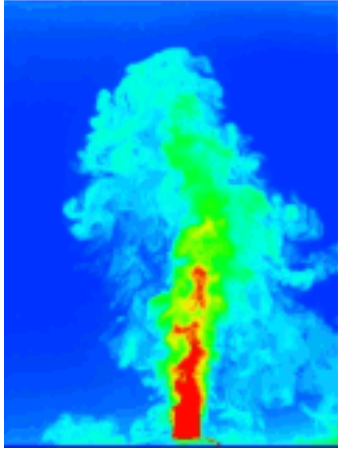
This article was downloaded by: [University of Maryland College Park]

On: 11 February 2011

Access details: Access Details: [subscription number 930842800]

Publisher Taylor & Francis

Informa Ltd Registered in England and Wales Registered Number: 1072954 Registered office: Mortimer House, 37-41 Mortimer Street, London W1T 3JH, UK



Journal of Turbulence

Publication details, including instructions for authors and subscription information:

<http://www.informaworld.com/smpp/title~content=t713665472>

Chasing eddies and their wall signature in DNS data of turbulent boundary layers

Clara O'Farrell^a; M. Pino Martín^a

^a Mechanical and Aerospace Engineering Department, Princeton University, Princeton, NJ, USA

First published on: 01 January 2009

To cite this Article O'Farrell, Clara and Martín, M. Pino(2009) 'Chasing eddies and their wall signature in DNS data of turbulent boundary layers', Journal of Turbulence, Volume 10, Art. No. N 15,, First published on: 01 January 2009 (iFirst)

To link to this Article: DOI: 10.1080/14685240902852701

URL: <http://dx.doi.org/10.1080/14685240902852701>

PLEASE SCROLL DOWN FOR ARTICLE

Full terms and conditions of use: <http://www.informaworld.com/terms-and-conditions-of-access.pdf>

This article may be used for research, teaching and private study purposes. Any substantial or systematic reproduction, re-distribution, re-selling, loan or sub-licensing, systematic supply or distribution in any form to anyone is expressly forbidden.

The publisher does not give any warranty express or implied or make any representation that the contents will be complete or accurate or up to date. The accuracy of any instructions, formulae and drug doses should be independently verified with primary sources. The publisher shall not be liable for any loss, actions, claims, proceedings, demand or costs or damages whatsoever or howsoever caused arising directly or indirectly in connection with or arising out of the use of this material.

Chasing eddies and their wall signature in DNS data of turbulent boundary layers

Clara O'Farrell and M. Pino Martín*

*Mechanical and Aerospace Engineering Department Princeton University,
Princeton, NJ, USA*

(Received 26 August 2008; final version received 15 February 2009)

We present an automated and physically rooted method to identify and temporally track hairpin packets and their wall signatures in direct numerical simulation data of turbulent boundary layers. Statistical tools and pattern-recognition algorithms are combined to identify the coherent structures and their signature on the wall, and object segmentation and feature-tracking algorithms are assessed and enhanced to achieve automatic monitoring of the temporal evolution of individual packets and their wall signatures. The visualization algorithms are validated against the statistical analysis. We demonstrate that the average geometric packet is representative of strong statistical ones. Satisfactory results are presented for the canonical case of an isolated hairpin packet convecting in channel flow, and for fully turbulent boundary layers. The method is also suitable for use in combination with experimental particle image velocimetry (PIV) data.

Keywords: turbulence; boundary layer; hairpin packet; DNS

1. Introduction

Although turbulence is chaotic in nature and may hence appear to lack an organized structure, turbulent flows have been found to exhibit certain coherent structures. Regarding wall-bounded turbulence, in a 1991 review article, Robinson [1] provided an overview of evidence of the existence of coherent structures, and more recently Ringuette, Wu and Martín [2], Ganapathisubramani, Longmire and Marusic [3], Adrian, Meinhart and Tomkins [4] and others have found evidence of coherent structures in direct numerical simulation (DNS) and experimental data. These structures have been the subject of much research over the past decades, and several models of wall turbulence have been proposed. In recent years, a growing consensus has emerged for a model based on Theodorsen's hairpin vortex model.

In 1952, Theodorsen [5] was the first to postulate the existence of a horseshoe or hairpin vortex, a simple flow structure whose presence explains both the formation of low-speed streamwise streaks and the ejection of near-wall low-momentum fluid into higher momentum regions farther from the wall [4].

In 1981, Head and Bandyopadhyay [6] visualized the stacking of individual hairpins into larger structures in turbulent boundary layers over a large range of Reynolds numbers

*Corresponding author. Email: pmartin@princeton.edu

($500 < Re_\theta < 17,500$). They concluded that the boundary layer consists of hairpin or horseshoe vortices that are inclined with a 45° downstream angle to the wall. Furthermore, they observed that hairpin vortices stacked into packets whose heads describe an envelope inclined at a 15° – 20° downstream angle. In addition, Head and Bandyopadhyay observed a variation in hairpin geometry with increasing Re_θ . At high Reynolds numbers ($Re_\theta > 2000$) they found hairpins with elongated vortex legs. In contrast, at low Reynolds numbers ($Re_\theta < 800$), they found hairpin vortices that were not elongated and were better described as horseshoes or vortex loops.

In 2000, Adrian, Meinhart and Tomkins [4] performed particle image velocimetry (PIV) in boundary layers and identified packets of hairpins that appeared regularly throughout the flow. From their results, Adrian et al. [4] postulated that hairpin packets consist of groups of hairpin structures moving at the same velocity relative to the mean flow. In the hairpin packet model of Adrian et al. [4], the hairpins in a packet are seen to align in the streamwise direction in a ramp-like formation at an angle γ to the wall. Packets enclose regions of low-momentum fluid induced by their counter-rotating legs, and align in the streamwise direction, giving rise to the low-momentum streaks observed by Ganapathisubramani, Longmire and Marusic [3], Hutchins and Marusic [7], Delo, Kelso and Smits [8] and Kim and Adrian [9] among others. Furthermore, Adrian et al. [4] postulated that hairpin packets evolve and grow in size, and eventually give rise to smaller, younger, slower packets, thus resulting in a nested hierarchy of packets. Adrian et al. [4] also noticed that most naturally occurring hairpins show a degree of asymmetry and are often cane-like in appearance. Following this work, the term ‘hairpin’ is used throughout to refer both to symmetric and asymmetric cane-like vortices, and includes both the elongated hairpins and the horseshoes or vortex loops found at different Reynolds number by Head and Bandyopadhyay [6].

In 2006, Martín, Smits, Wu and Ringuette [10] were able to show the temporal evolution of a hairpin packet in turbulent flow over a compression corner. They identified three hairpins belonging to a packet by visual inspection, and then identified these same hairpins in later frames.

Although the identification of hairpins and hairpin vortices has been accomplished, manually tracking these structures is time consuming. The study of hairpin packet formation, evolution, interaction and influence on flow features (such as the wall shear stress and wall pressure) requires sophisticated, reliable and automated tools for packet identification. In this paper, we describe an automated and scientifically rooted method to identify and temporally track hairpin packets and their wall signatures (as described in Section 3) in three-dimensional space and time DNS data of turbulent boundary layers. Statistical tools and pattern recognition algorithms are used to identify hairpin packets and their wall signature, and object segmentation and feature-tracking algorithms are assessed and enhanced to achieve the monitoring of the temporal and spatial evolution of packets and their wall signatures. The paper is organized as follows: Sections 2 and 3 describe the criteria for identifying hairpin packets and their wall signatures in terms of a geometric algorithm and statistical analysis. Section 4 describes the relationship between the geometric and statistical packet identification techniques. Section 5 describes the object segmentation and feature tracking algorithms. Section 6 presents the tracking of a single, synthetically generated hairpin vortex in DNS data and Section 7 presents similar results from fully turbulent boundary layer DNS data. Conclusions are presented in Section 8.

2. Identifying hairpin vortices and hairpin packets

Vortex identification criteria rely on definitions of the vortex that are more mathematical in nature than those described above. One such definition is provided by Robinson, Kline and Spalart [1]:

A vortex exists when instantaneous streamlines mapped onto a plane normal to the vortex exhibit a roughly circular or spiral pattern, when viewed from a reference frame moving with the center of the vortex core.

Several criteria for identifying structures consistent with this description have been proposed. Taylor, Martín and Smits [11] compared the performance of three such criteria: The discriminant of the velocity gradient tensor criterion suggested by Chong, Perry and Cantwell [12], the swirling strength criterion postulated by Zhou, Adrian, Balachandar and Kendall [13] and the Hessian of pressure criterion suggested by Jeong and Hussain [14]. Taylor et al. [11] found that the three criteria gave nearly identical results for supersonic turbulent boundary layers.

Following Zhou et al. [13], Ringuette et al. [2] used the swirling strength as the primary criterion for vortex identification in their study of hairpin packets in DNS data. They showed that it is possible to identify hairpin vortices and hairpin packets and determine average package properties in DNS data of compressible boundary layers. The authors used iso-surfaces of swirling strength to visualize vortex structures and devised an algorithm that singled out hairpins and hairpin packets using their geometric properties. In contrast, Green, Rowley and Haller [15] used direct Lyapunov exponents (DLE) as a tool for identifying hairpin vortices in DNS data. They performed this analysis in a single synthetically generated hairpin vortex evolving into a packet described by Zhou et al. [13] and showed that the DLE analysis is in close agreement with the swirling strength criterion.

The DLE is an integrative technique, which is powerful in identifying the most dominant structure present. It, however, cannot be used to study the local instantaneous fluid interactions. For this reason, we chose to employ the instantaneous geometric algorithm in the present study. Further details about the swirling strength criterion and the geometric algorithm are given below.

2.1. Visualization of vortex structures

In this study, iso-surfaces of swirling strength are used as the primary criterion for vortex identification, following Zhou et al. [13] and Ringuette et al. [2]. The swirling strength (λ_{ci}^2) is defined as the square of the imaginary component of the eigenvalues of the velocity gradient tensor. A formal description of the swirling strength is given in Zhou et al. [13] and is summarized here.

The velocity (\vec{u}) gradient tensor is denoted by the 3×3 real matrix A , where

$$A = \nabla \vec{u} = \begin{bmatrix} \frac{\partial u}{\partial x} & \frac{\partial u}{\partial y} & \frac{\partial u}{\partial z} \\ \frac{\partial v}{\partial x} & \frac{\partial v}{\partial y} & \frac{\partial v}{\partial z} \\ \frac{\partial w}{\partial x} & \frac{\partial w}{\partial y} & \frac{\partial w}{\partial z} \end{bmatrix}. \quad (1)$$

Then the characteristic equation of A is

$$\lambda^3 + P\lambda^2 + Q\lambda + R = 0 \quad (2)$$

where

$$P = -tr(A) \quad (3)$$

$$Q = \frac{1}{2}[P^2 - \text{tr}(AA)] \quad (4)$$

$$R = \frac{1}{3}[-P^3 + 3PQ - \text{tr}(AAA)]. \quad (5)$$

Substituting $\lambda = \tilde{\lambda} - \frac{1}{3}P$ Equation (2) becomes

$$\tilde{\lambda}^3 + \tilde{Q}\tilde{\lambda} + \tilde{R} = 0 \quad (6)$$

where $\tilde{Q} = Q - \frac{1}{3}P^2$ and $\tilde{R} = R + \frac{2}{27}P^3 - \frac{1}{3}PQ$. The discriminant of A is then

$$\Delta = \left(\frac{1}{3}\tilde{Q}\right)^3 + \left(\frac{1}{2}\tilde{R}\right)^2. \quad (7)$$

When $\Delta > 0$, A will have one real eigenvalue and a complex conjugate pair of eigenvalues, and when $\Delta \leq 0$ all three eigenvalues are real. Although Chong et al. [12] claim that Δ being strictly greater than zero is a sufficient condition for determining the presence of a vortex, Zhou et al. [13] examined the eigenvalues of A . Letting λ_{ci} be the imaginary component of the complex eigenvalues of A then the swirling strength (λ_{ci}^2) becomes

$$\lambda_{ci}^2 = \frac{3}{4} \left[\left(\frac{1}{2}\tilde{R} + \sqrt{\Delta} \right)^{\frac{1}{3}} - \left(\frac{1}{2}\tilde{R} - \sqrt{\Delta} \right)^{\frac{1}{3}} \right]^2. \quad (8)$$

The eigenvalues of the velocity gradient tensor characterize the fluid's local velocity, and the existence of a pair of complex eigenvalues of $\nabla\vec{u}$ therefore indicates a spiraling motion consistent with the presence of vortices. Furthermore, Zhou et al. [13] have remarked that the strength of the local swirling motion is quantified by λ_{ci} , and hence this criterion is referred to as the 'swirling strength'.

The swirling strength criterion distinguishes between rotations caused by isolated vortex cores and angular deformation caused by shear layers, so it can be used to filter out shear layers. It does not, however, differentiate between in-plane rotation in the clockwise and counter-clockwise directions, so it cannot differentiate between regions where direction of rotation is consistent with Theodorsen's hairpin model and regions where the direction of rotation is inconsistent with this model.

2.2. Geometric identification of hairpin packets

Ringuette, Wu and Martín [2] developed a method for finding hairpin packets in DNS data for turbulent boundary layers and characterizing their average properties. They developed an algorithm that searched streamwise-wall-normal (x - z) planes for hairpin vortex 'heads' that were grouped together into ramp-like structures that formed a shallow downstream angle with the wall. These criteria are consistent with the hairpin packet model of Adrian et al. [4], and with the experimental results of Head and Bandyopadhyay [6] and Brown and Thomas [16]. Ringuette et al. [2] used their packet-finding scheme to analyze data for a Mach 3

turbulent boundary layer with $Re_\theta = 2390$ and determined the average package properties. The authors found that hairpin packets, on average, were inclined with a downstream angle to the wall of approximately 20° , spanned approximately 0.4δ in the streamwise direction, and convected with a speed of $0.7U_\delta$, where δ and U_δ are the boundary-layer edge and the boundary-layer-edge velocity, respectively. These results are in agreement with those of Adrian et al. [4], Ganapathisubramani et al. [3] and Head and Bandyopadhyay. In this paper, we use the geometric hairpin packet identification scheme of Ringuette et al. [2], which is briefly summarized below.

At every plane, the authors used both the swirling strength (λ_{ci}^2) and the vorticity (ω) as criteria for identifying potential vortex heads. The swirling strength was used to filter out shear layers, and the vorticity was used to distinguish between regions of large, positive out-of-plane vorticity, which are consistent with Theodorsen's model, and regions of large, negative out-of-plane vorticity which are not. As a result, at every plane the authors identified those regions where λ_{ci}^2 exceeded $4.5\bar{\lambda}_{ci}^2$ (where, the overbar indicates the mean) and the out-of-plane vorticity exceeded the mean by at least two standard deviations, considering only regions that lie between the buffer region (defined as $z^+ = 30$) and the boundary layer edge (defined where $u = U_\delta \equiv 0.985U_o$, and U_o is the free stream velocity). These regions were marked as potential hairpin head vortices.

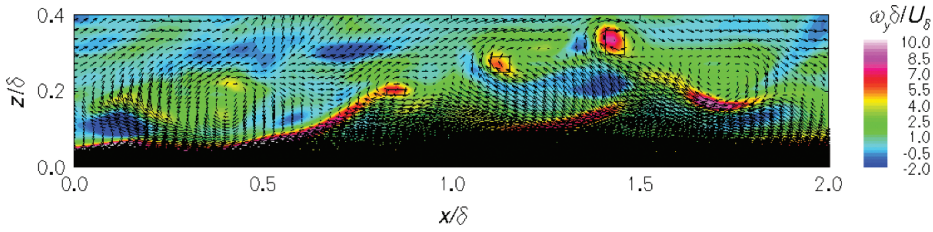
These criteria were seen to occasionally select structures that were too large to be hairpin head vortices and were most likely hairpin vortex legs, so a size threshold was introduced. Ringuette et al. [2] used a maximum size criterion of $0.1\delta \times 0.1\delta$ and categorized all larger structures as legs. These 'legs' may be attached below a hairpin head, so the authors investigated these structures to determine whether they could be partitioned into a head and leg, and reclassified any heads they found as such.

Once the locations of hairpin head vortices were determined, Ringuette et al. [2] used geometric criteria consistent with the model of Adrian et al. [4] to group the head vortices into packets. The head vortex that was closest to ($x = 0$, $z^+ = 30$) was chosen as the reference head vortex for the first packet, and the algorithm then searched the remaining head vortices that were within a streamwise distance of 0.5δ and formed an angle between 0° and 45° with the reference head vortex. If one such vortex was found, it was identified as forming a packet with the reference vortex and was taken as the new reference head vortex for the packet. This process was repeated until all vortices belonging to the first packet were identified. Then the search proceeded to the next packet until all head vortices were grouped into their respective packets.

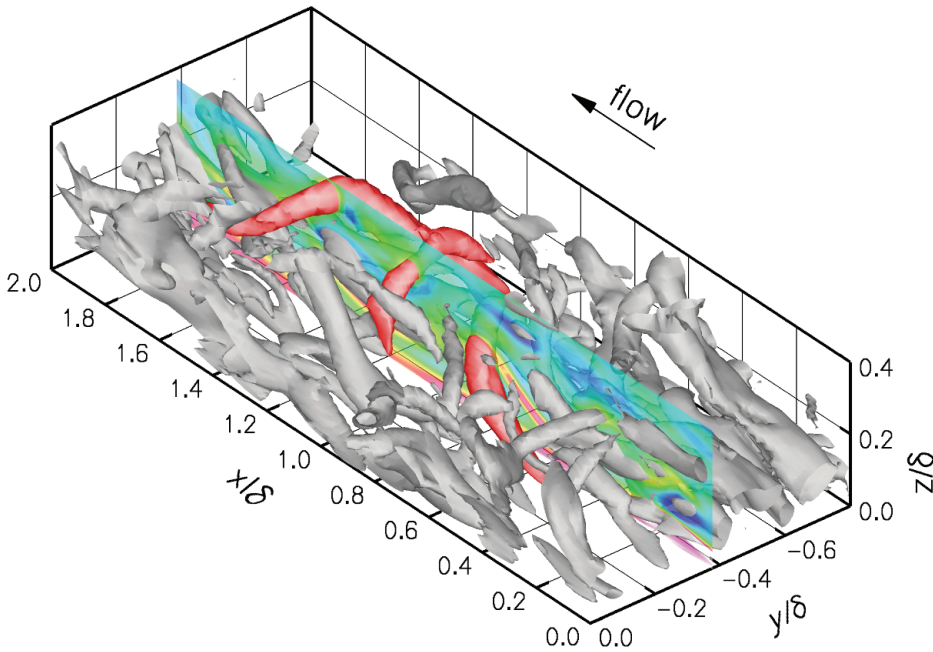
Figure 1(a) from Ringuette et al. [2] shows the results of running the geometric identification algorithm on one x - z plane of DNS data for a Mach 3 turbulent boundary layer with $Re_\theta = 2390$. The black rectangles mark the three head vortices that have been identified as belonging to the same packet by their geometric properties. As expected, they are aligned with a shallow downstream angle relative to the wall. Figure 1(b) [2] shows the same packet visualized in three dimensions using iso-surfaces of swirling strength. The geometric algorithm of Ringuette et al. [2] performs well when identifying hairpins and hairpin packets that are consistent with Adrian et al.'s [4] model in fully turbulent boundary layer data.

3. The wall signatures of hairpin packets

Several experiments (Brown & Thomas [16, 17], Thomas & Bull[18]) and numerical simulations (Ringuette et al. [2], Ahn, Graham & Rizzi [19], Kasagi, Suzuki & Iida [20]) have found patterns in the wall shear, wall pressure and correlations between wall shear and



(a)



(b)

Figure 1. Geometric packet identification from Ringuette, Wu and Martín [2] in DNS data of turbulent boundary layers. (a) shows a streamwise wall-normal slice containing a hairpin packet. Contours show spanwise vorticity, vectors show velocity with $0.69U_\delta$ subtracted from u . Three hairpin heads have been identified and highlighted using black rectangles. (b) shows the same packet visualized using iso-surfaces of swirl strength, where the hairpins in the packet have been highlighted in red.

velocity that are indicators of the presence of organized structures in the boundary layer. These characteristic patterns in the flow properties at the wall induced by hairpin packets are collectively referred to as the wall signatures of hairpin packets. Such signatures can be used to identify and track hairpin packets.

In a 1977 experiment, Brown and Thomas [16, 17] monitored the shear stress at the wall and the velocity at several points from the wall to identify large-scale organized structures. Using an array of hot wires and a wall shear stress probe, they measured the correlation between shear stress at the wall and velocity in turbulent boundary layers. This analysis

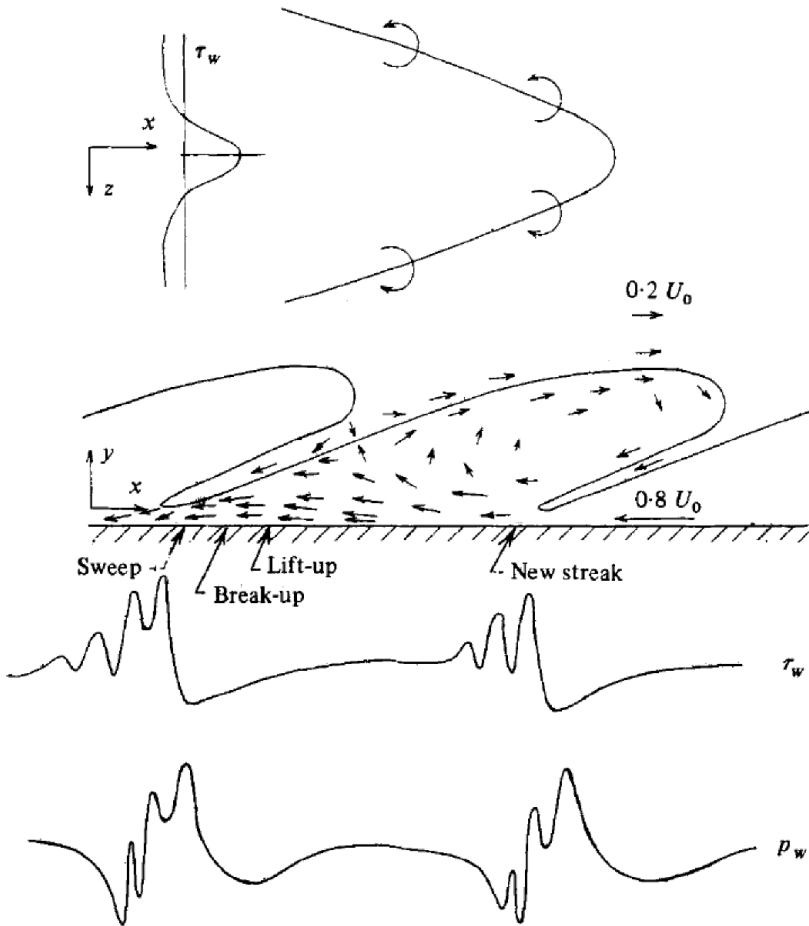


Figure 2. Model of organized structures in turbulent boundary layers from Thomas and Bull [18], after Brown and Thomas [16], as seen by an observer moving at $0.8U_0$.

allowed them to detect the presence of large structures that are inclined with a shallow (18°) downstream angle relative to the wall, which is consistent with the results of Head and Bandyopadhyay [6] and the hairpin packet model of Adrian et al. [4]. Additionally, studying the evolution of the wall shear stress led Brown and Thomas [16, 17] to conclude that these large-scale structures also induce small-scale wall shear stress fluctuations that convect with the organized structure. Burton [21], Willmarth [22] and Thomas and Bull [18] also found a characteristic signature in the wall pressure fluctuations that is associated with the presence of a large structure in the boundary layer. Figure 2 is a schematic from Thomas and Bull [18] showing the large structure and associated wall shear and wall pressure distributions.

In the present work, we use the wall shear stress and velocity correlation analysis as a criteria to identify and track strong packets. Regions of the wall where such correlations are elevated are interpreted as signatures indicating the presence of a hairpin packet. The Brown and Thomas [16] correlation analysis is briefly described below.

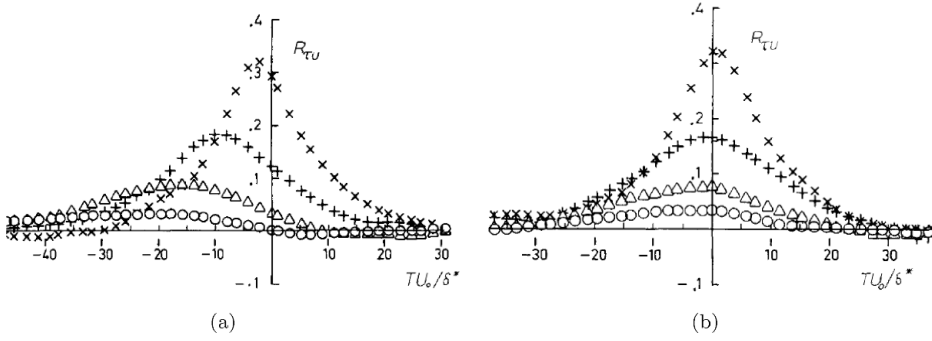


Figure 3. Correlations between wall shear stress and velocity versus time delay at various wall-normal locations from Brown and Thomas [16]. \times , $y/\delta = 0.05$; $+$, $y/\delta = 0.25$; Δ , $y/\delta = 0.50$; \circ , $y/\delta = 0.75$.

3.1. Wall shear stress and velocity correlations

Brown and Thomas [16] calculated the long-time averaged correlation between the shear stress at a point at the wall and the velocity at a certain distance from the wall

$$R_{\tau_w u}(T) = \lim_{T_s \rightarrow \infty} \int_0^{T_s} \tau_w(t)u(t+T)dt, \quad (9)$$

where $\tau_w(t)$ is the shear stress at the wall at time t and $u(t+T)$ is the streamwise velocity at time $t+T$, where T is a nondimensional time delay. Figure 3(a) shows their results when the hot wires were stacked vertically directly above the hot film. Notice how the correlations peak at increasing time delay as the probes are moved farther from the wall. To obtain the plot in Figure 3(b), the authors varied the streamwise location of the hot wires until the correlation peaked at zero time delay. The locations that yielded correlation maxima at zero were found to form an 18° angle with the wall.

Ringuette et al. [2] were able to perform a similar analysis on DNS data for turbulent boundary layers. They calculated the correlation between the shear stress at a point at the wall and the velocity at a certain distance from the wall using

$$R_{\tau_w u}(\Delta x) = \frac{1}{(x_2 - x_1)} \left\langle \overline{\int_{x_1}^{x_2} \tau'_w(x)u'(x + \Delta x)dx} \right\rangle / \tau'_{w,RMS}u'_{RMS}, \quad (10)$$

where the overbar and angle brackets indicate spatial (streamwise and spanwise) and temporal averaging, respectively. Figure 4 shows the results from Ringuette et al. [2]. Figure 4(a) shows standard correlations, while Figure 4(b) shows the 'enhanced' correlations, obtained by conditionally averaging the instances in which the correlation at $z/\delta = 0.25$ was greater than 0.3 at the peak Δx location shown in Figure 4(a). The results shown in Figure 4 were found to agree with those of Brown and Thomas [16].

In the present work, we use Equation. 10 without the averaging to determine the correlation coefficient profiles between the shear stress at the wall and the velocity, for each point at the wall. We use a correlation width that is large enough for both the correlations to fall below 0.2. The regions where the maximum value of this correlation at a distance of 0.2δ from the wall exceeded five times the average correlation coefficient are identified.

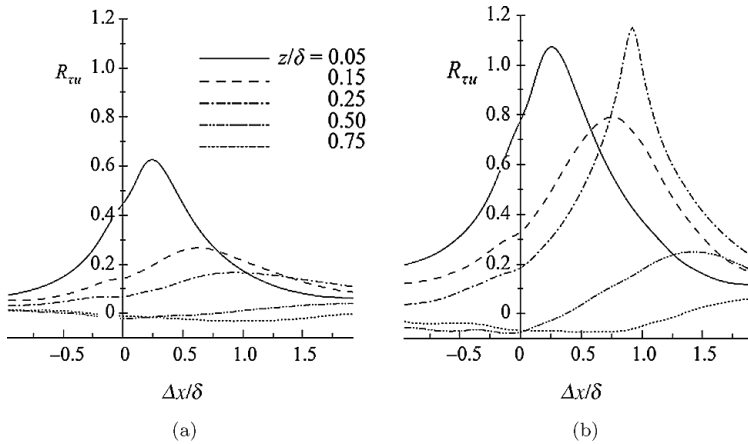


Figure 4. Correlations between wall shear stress and velocity versus streamwise distance at various wall-normal locations from Ringuette, Wu and Martín [2]. (a) Standard correlations, and (b) ‘enhanced’ correlations.

These areas constitute the wall signatures of ‘strong’ packets, indicating a ‘strong’ event such as a turbulent burst in the lower part of the boundary layer.

4. Relationship between the geometric algorithm and the correlation method

We determine profiles of the convection velocity for vortices belonging to hairpin packets using both the geometric algorithm and the ‘enhanced’ correlation data. For the geometric algorithm, the convection velocity of a single vortex in a packet is computed by averaging u at each grid point within the vortex; the value is then associated with a wall-normal location corresponding to the vortex core, assumed to be maximum for the vortex λ_{ci} .

For the ‘enhanced’ correlation method, we obtain the packet convection velocity at the eleven wall-normal distances by computing the correlation profiles between u and the shear stress at each (x, y) wall location (no spanwise or streamwise averaging). If the correlation peak at $z/\delta = 0.2$ indicates a ‘strong’ event, the streamwise velocity u is sampled at the $(x + \Delta x, z)$ peak location of the correlation profile at each of the eleven wall-normal distances. The results at each z -location are averaged together. The $(x + \Delta x, z)$ peak locations can be thought of as lying within the back of the ramp-like structure associated with each instantaneous strong event. We present the ‘enhanced’ correlation and geometric-algorithm data spanwise averaged over all planes.

Essentially, statistics on the average packet structure can be found using the correlation analysis of Brown and Thomas [16] and the data can be categorized into average-strong, average-average, and average-weak packets. In contrast, the geometric algorithm identifies only the subset of packets that conforms with an ideal geometric criteria. When the geometric analysis is combined with the correlation analysis, the geometric events can also be decomposed into average strong-geometric, average-geometric, and weak-geometric packets. Figure 5 plots the averaged vortex convection velocity and the mean flow velocity profiles for the Mach 3 and $Re_\theta = 2390$ data [23], given by the geometric analysis combined with the correlation analysis. For reference, the average convection velocity of strong packets given solely by the correlation analysis is also plotted, along with the mean

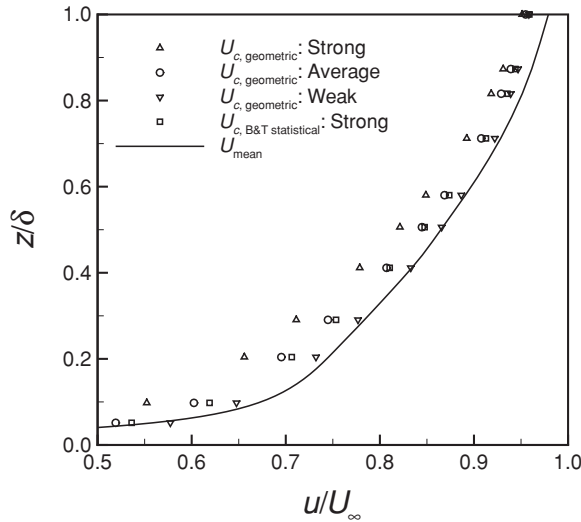


Figure 5. Vortex convection velocity profiles, with the mean velocity profile in the solid line. The use of ‘geometric events’ at the wall limit the correlation analysis to regions where ideal hairpin packets have been found, which corresponds to the first three legend entries. The convection velocity determined from the ‘strong’ Brown and Thomas [16] correlation is plotted as a square symbol.

velocity profile. The data suggest that the average geometric packet is representative of strong statistical packets.

5. Tracking scheme

We use a combination of geometric [2] and statistical methods [16], as well as the object segmentation and feature tracking routines developed by Wang and Silver [24] to identify hairpin packets and track them temporally and spatially in DNS data of turbulent boundary layers.

5.1. Identification of strong packets

The Ringuette et al. [2] analysis is applied to every volume of DNS data. At every plane, we identify the hairpin head vortices and group them into packets based on the geometric criteria consistent with the model of Adrian et al. [4]. By performing this analysis, we are able to recover all of the transverse hairpin head vortices that belong to a hairpin packet. When performing the in-plane analysis, however, the algorithm discards elongated structures that could potentially be hairpin legs.

We are interested in identifying and tracking a handful of strong packets. Following the analysis of Brown and Thomas [16], we interpret regions where the correlation between τ_w and ρu is elevated as signatures indicating the presence of a strong hairpin packet, and only those packets identified by the geometric criteria and whose location corresponds with the presence of a Brown and Thomas [16] wall signature are selected for tracking.

We find that the streamwise location of the wall signatures corresponds closely with the streamwise location of the vortex legs of hairpins in strong packets, and that the signatures are offset slightly from these elongated vortex legs in the spanwise direction. We use these two facts, along with the condition that λ_{ci}^2 exceed $4.5\bar{\lambda}_{ci}^2$ to reconstruct the vortex legs of the hairpins in strong packets.

5.2. Tracking software

We are interested in tracking each packet to observe its evolution. This is achieved by using the object segmentation and feature tracking algorithms developed by Wang and Silver [24] and implemented in the Object Segmentation and Feature Tracking (Ostrk2.0) package [25].

Ostrk2.0 is a software package for Advanced Visual Systems/Express (AVS), a program that serves as a platform for building applications to process and visualize complex data sets. The Ostrk2.0 package allows users to track objects in sequential data sets with similar grid coordinates, each one representing a single time step or frame. The data sets must contain data corresponding to a single variable (such as λ_{ci}^2), which is used to compute iso-surfaces at a user-specified threshold. The object segmentation and feature-tracking algorithms are then applied to these iso-surfaces.

The Ostrk2.0 package performs two routines on the data sets: Object segmentation and feature tracking. During the object segmentation routine, each connected object in a plot of iso-surfaces of swirling strength is identified as a separate object. The outcome of the object segmentation routine is therefore dependent on the threshold value used to generate the iso-surface, which is entered by the user as a percentage of the maximum value of the swirling strength in the first frame. This value is used in all subsequent data sets for the generation of iso-surfaces. An a priori knowledge of a suitable threshold value is therefore required.

Each connected object identified by the object segmentation routine is given a unique object identification number (object ID), and its geometric properties are stored. Between calls to the object segmentation routine for different data frames, the feature tracking routine is called. The feature tracking routine links every object ID in a given frame to an object ID in the preceding frame, thus recording the evolution of each object. The algorithm used to perform this task was also designed by Wang and Silver [24]. It employs a minimum geometric difference scheme in a recursive octree algorithm to determine the most likely predecessor(s) of each object. The algorithm recognizes the creation of new objects, the merging of objects and their split and dissipation. The object histories are output in a single *.trakTable file, and the geometric properties of the objects in each frame are output in *.poly and *.uocd files corresponding to each frame.

In this study we are interested in tracking the evolution of strong hairpin packets. Thus, all other vortices are removed from the dataset by setting the value of λ_{ci}^2 to zero for all points not belonging to strong packets. A threshold of $\lambda_{ci}^2 = 4.5\bar{\lambda}_{ci}^2$ is then specified to generate an iso-surface of λ_{ci}^2 that contains only the strong hairpin packets. Ostrk2.0 is then applied to this iso-surface to track the evolution of the strong packets in sequential data frames.

5.3. Analysis of tracking results

The results of tracking Ostrk2.0 are output as a single *.trakTable file containing the history of each object Ostrk identified and a series of files (including *.poly and *.uocd files) containing information about the objects at each single time step.

In Ostrk2.0's *.poly files, each object is defined as a polygon. These files can be viewed in AVS with the help of a specialized module, and can be modified to change the color of specific polygons or even remove them altogether. The *.poly files generated by Ostrk2.0 were therefore used to create new *.poly files where the relevant vortices are highlighted in particular colors, or where all other vortices have been removed. These new *.poly files were then visualized using AVS.

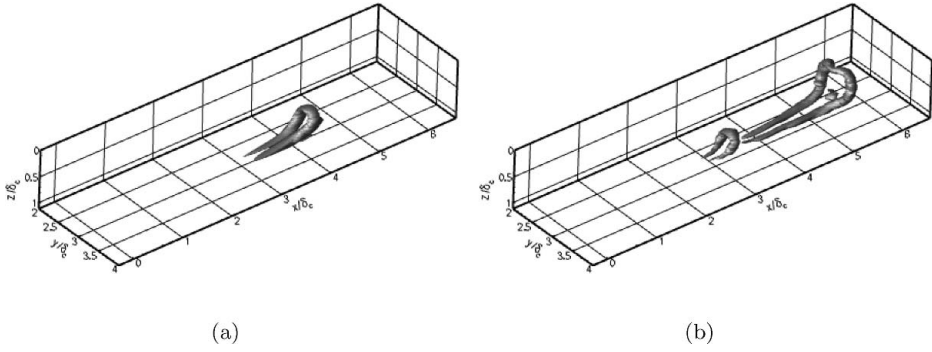


Figure 6. Evolution of a single hairpin in a channel. Iso-surfaces of swirling strength show the hairpin in its early stages (a) and after it has spawned a new hairpin (b). [Click here to watch the corresponding movie.](#)

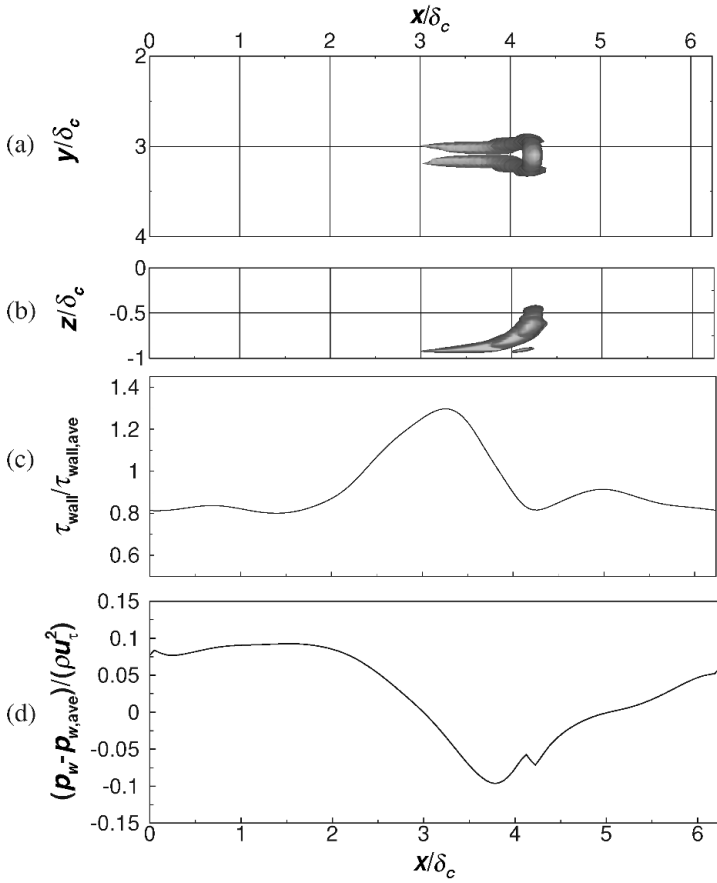


Figure 7. Evolution of the wall shear and wall pressure signals. (a) and (b) show the position of the hairpin using iso-surfaces of swirl strength. (c) shows the wall shear along a streamwise line at $y/\delta_c = 2.97$, (d) shows the wall pressure along a streamwise line at $y/\delta_c = 2.97$.

Ostrk2.0's *.uocd file contains information about each object in a given frame, including which points in the original data set comprise it and the values of λ_{ci}^2 at each of these points. These files therefore provide the information that allowed us to export the results of the tracking into Tecplot for further processing, and even allowed to export modified data sets in which only a portion of the objects were included.

6. A canonical case

We first consider a simple canonical flow consisting of a single isolated hairpin convecting in incompressible channel flow. The DNS database is from Green, Rowley and Haller [15], who extracted a hairpin from a DNS of a fully developed turbulent channel flow at Reynolds number based on wall friction velocity and channel half width of $Re_\tau = 180$, and used a flow field containing this vortex alone as the initial condition to their DNS solver. In this flow, we monitor the wall signature of the single hairpin using the wall-shear and wall-pressure signals, and the correlations between wall shear and velocity. This simple flow is perfectly

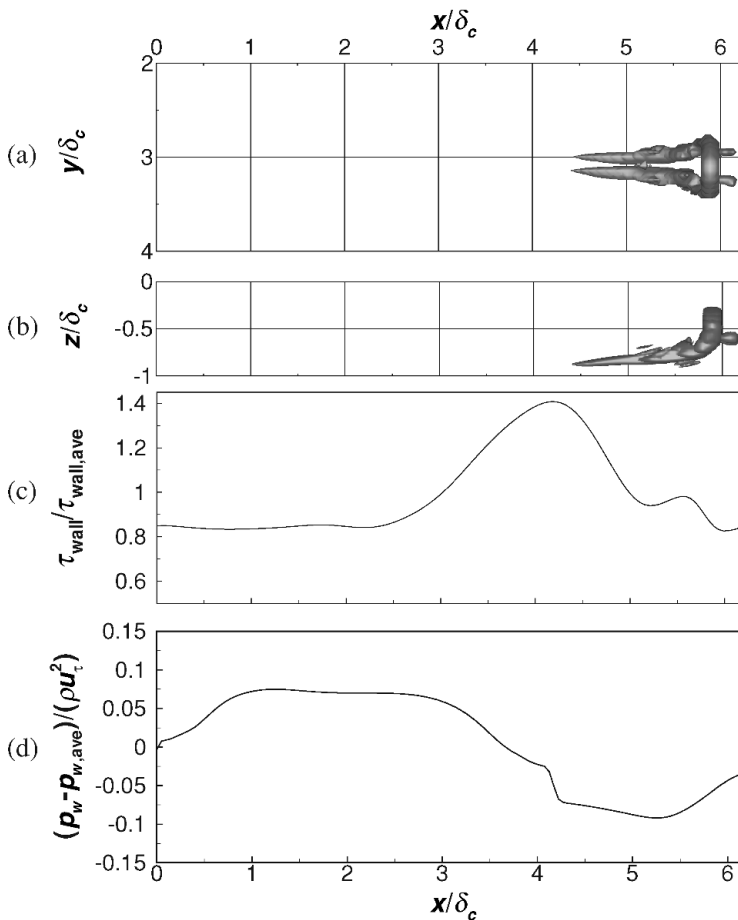


Figure 8. Evolution of the wall shear and wall pressure signals. (a) and (b) show the position of the hairpin using iso-surfaces of swirl strength. (c) shows the wall shear along a streamwise line at $y/\delta_c = 2.97$, (d) shows the wall pressure along a streamwise line at $y/\delta_c = 2.97$. Click here to watch the corresponding movie.

suites for testing the hypotheses concerning hairpin wall signatures presented earlier, since the simplicity of the data allows us to clearly identify a single hairpin's signature.

Figure 6(a) shows the iso-surface of λ_{ci}^2 at 10% of the maximum swirl value for the initial frame in the dataset. Here the hairpin is in the early stages of development. Figure 6(b) is a later frame showing the now mature primary hairpin, and the secondary hairpin it has spawned. The evolution of the hairpin and its development into a packet was recorded into an animation which is included with this study.

In Figure 7, distinct signatures in τ_w and p_w are seen to coincide with the streamwise and spanwise locations of the hairpin. Figures 7(b) also show iso-surfaces of λ_{ci}^2 (10% of the maximum swirl) at the initial frame from the (a) top and (b) side. Figure 7(c) shows τ_w along a line parallel to the direction of flow (the x-axis) at $y/\delta_c = 2.97$. The location of the line along which the wall shear was monitored corresponds to the spanwise alignment of the center of the hairpin. Comparing Figures 7(a–b) and Figure 7(c) show that a peak in τ_w coincides with streamwise location of the tip of the hairpin's vortex legs. A similar result was observed in the wall pressure signature along the same streamwise line. Figure 7(d) shows a decrease in p_w that corresponds with the streamwise location of the intersection between the hairpin's head and legs in Figures 7(a–b).

The results of Figure 7 are shown again in Figure 8, for a later frame. Figures 8(a–b) show that the hairpin has convected approximately $1.5\delta_c$ downstream. Figures 8(c–d) show that the peak in τ_w and well in p_w have convected downstream accordingly, so that their locations still correspond to the hairpin's position. The evolution of the hairpin and τ_w wall signature throughout the entire data set was recorded and is included as an animation.

A similar hairpin wall signature in the Brown and Thomas [16] correlation results is seen in Figure 9, which shows the location of wall regions where the value of the Brown and Thomas correlations exceeds five times the average correlation for the volume ($R_{\tau u} = 5\bar{R}_{\tau u}$).

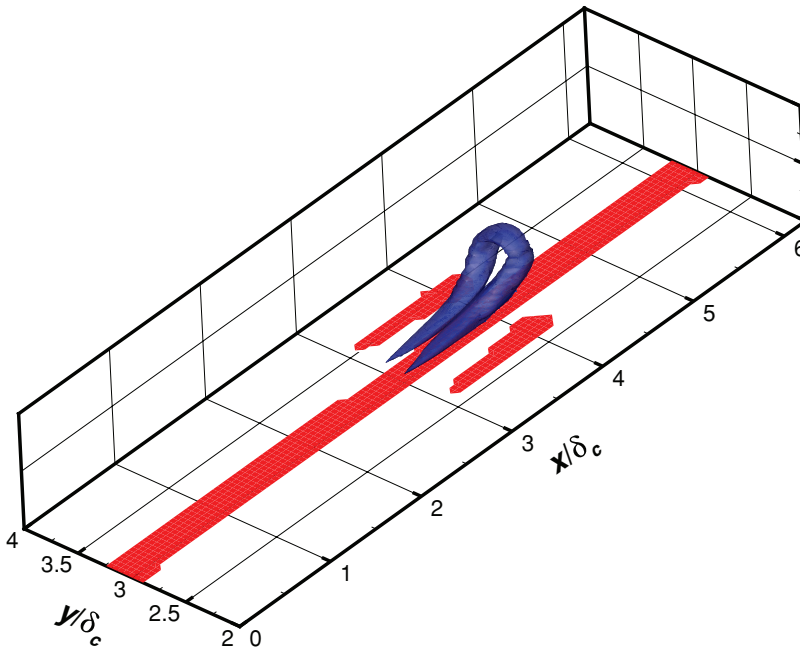
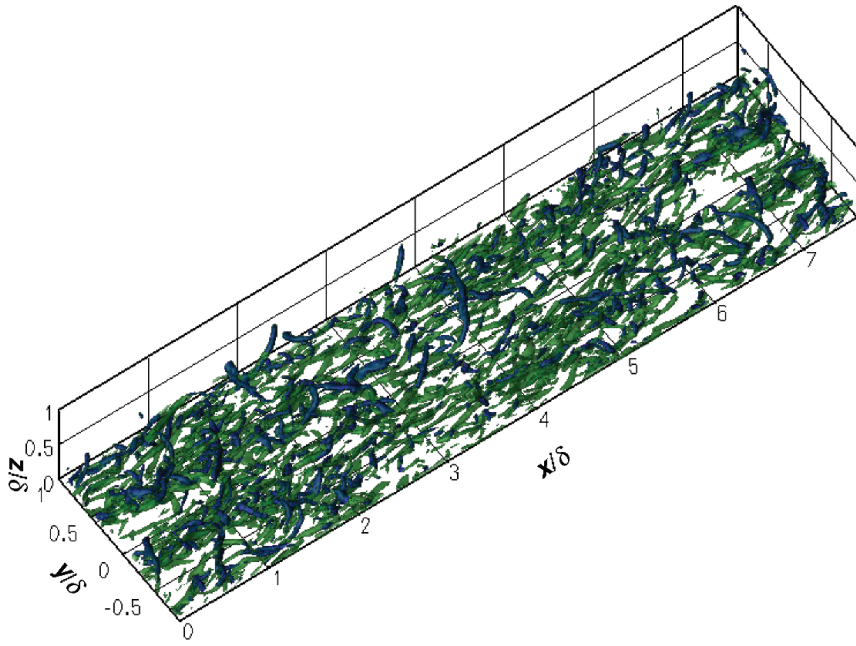
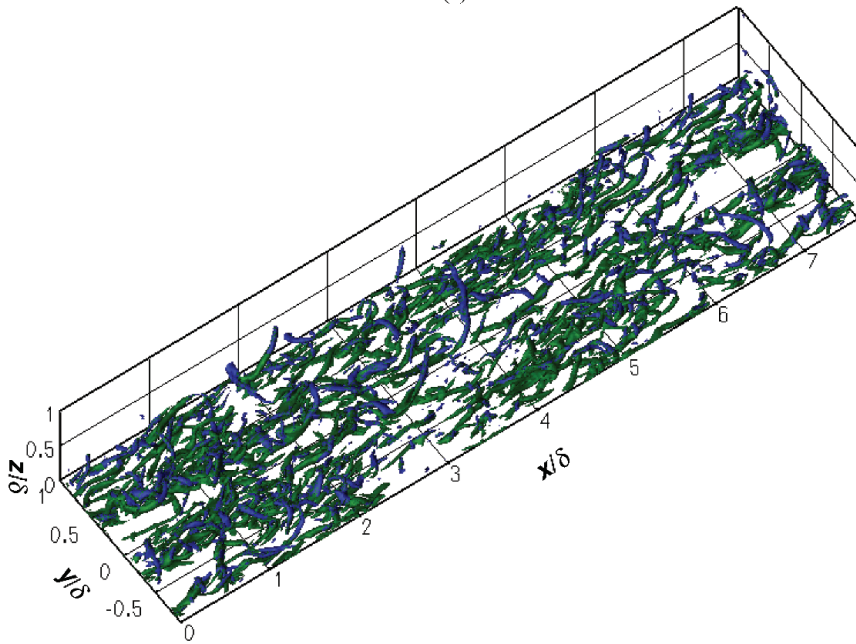


Figure 9. Wall signature corresponding to the hairpin's legs, determined using Brown and Thomas [16] correlations between velocity and shear stress. Regions where the correlation coefficient exceeds five times the average appear in red.



(a)



(b)

Figure 10. Pre-processing the input to the object segmentation routine in DNS data [23]. (a) Hairpin head vortices (the points identified by the packet finding algorithm) are visualized using an iso-surface of $\lambda_{ci}^2 = 4.5\lambda_{ci}^2$ (in blue). The original iso-surface of $\lambda_{ci}^2 = 4.5\lambda_{ci}^2$ is shown in green at 50% translucency for reference. (b) Hairpin head vortices are again visualized using an iso-surface of $\lambda_{ci}^2 = 4.5\lambda_{ci}^2$ (in blue), and the result of attempting to reconstruct their legs using an iso-surface of λ_{ci}^2 as the only criterion is shown in green using with an iso-surface of $\lambda_{ci}^2 = 4.5\lambda_{ci}^2$.

The regions of elevated correlation at the wall are shown in red, and an iso-surface of swirl showing the relative position of the hairpin is shown in blue. The two smaller red regions on either side of the volume centerline are signatures corresponding to each of the hairpin's legs, while the elongated region running through the center of the volume is a result of the volume being small in relation to the hairpin's size. Figure 9 shows that the streamwise location of the two signatures coincides with the streamwise location of the hairpin's vortex legs, but the signatures appear at either side of the hairpin in the spanwise direction.

7. Turbulent boundary layer

We use a DNS database of a boundary layer at Mach 3 and Reynolds number based on momentum thickness of $Re_\theta = 2300$ from Martín [23]. The methods described in the previous sections are used to identify strong hairpin packets and monitor their local evolution and wall signature.

Figure 10(a) shows an iso-surface of $\lambda_{ci}^2 = 4.5\bar{\lambda}_{ci}^2$ for the initial frame in the boundary layer database. The hairpin head vortices identified by the packet-finding geometric algorithm have been highlighted in blue, and all other vortices are shown in green at 50% translucency. Figure 10(b) shows the result of attempting to form the legs of the hairpin heads using an iso-surface of λ_{ci}^2 as the only criterion for reconstruction. Again, the hairpin head vortices have been visualized using an iso-surface of $\lambda_{ci}^2 = 4.5\bar{\lambda}_{ci}^2$ and highlighted in blue, and the tentative reconstructed legs are shown in green using an iso-surface at the same level. Comparing Figures 10(a) and 10(b) shows that λ_{ci}^2 is an insufficient criterion for reconstructing vortex legs, since most of the vortices in Figure 10(a) appear among the tentative reconstructed legs of Figure 10(b), regardless of their shape.

The wall signatures are combined with the result of the geometric packet-finding algorithm in order to identify 'strong' packets and recover their vortex legs. Figure 11 shows

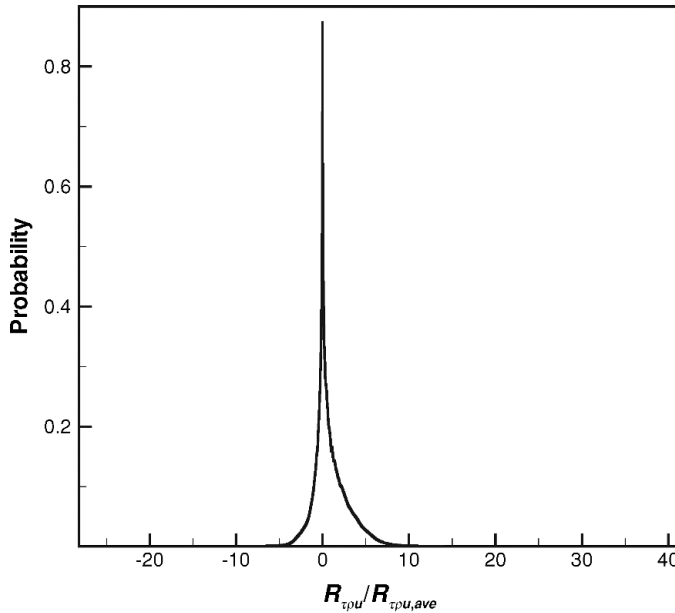
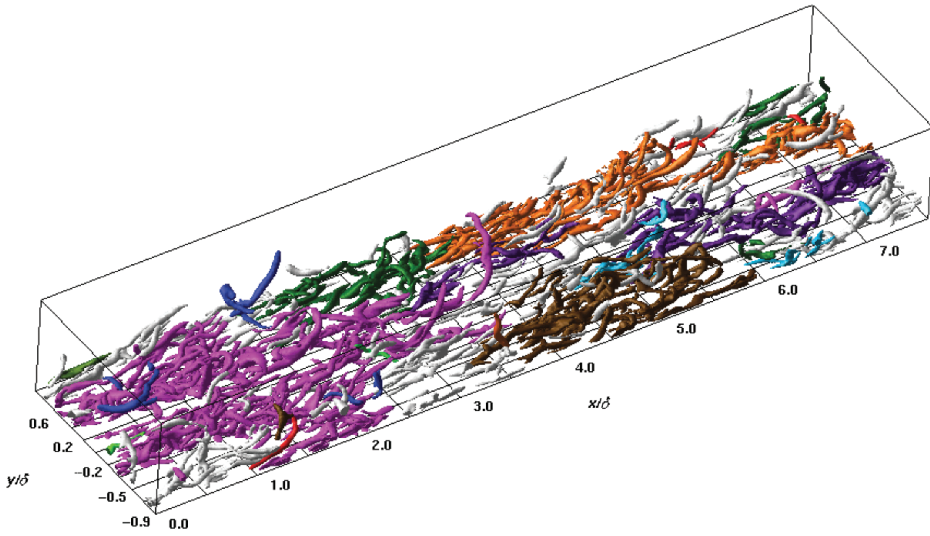


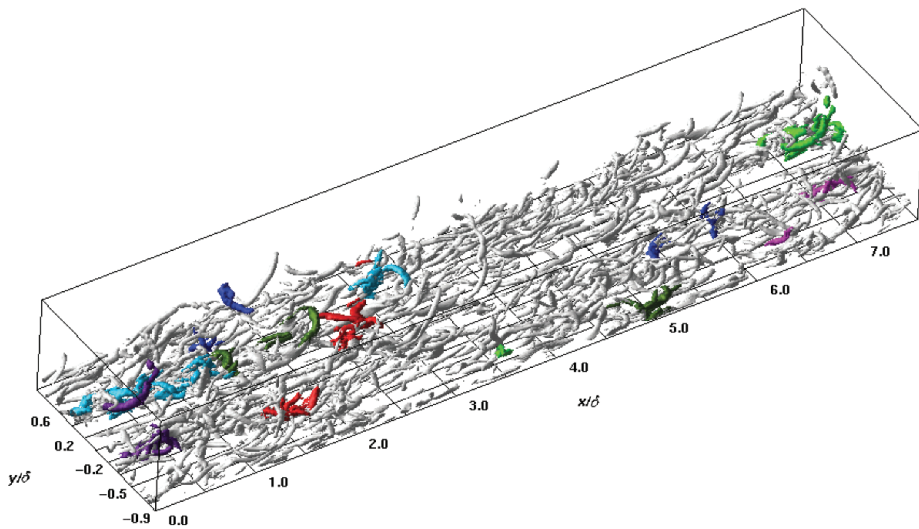
Figure 11. Probability density function of the normalized correlation coefficient between the wall stress and momentum, $R_{\tau\rho U} / R_{\tau\rho U,ave}$.

the probability density function (PDF) of the correlation coefficient $R_{\tau_w Du}$ (normalized by the average correlation R_{ave}). Regions where the correlation exceeds five times the average correlation represent less than 5% of all points on the wall, and were hence interpreted as the wall signatures of strong packets.

Figure 12 shows a comparison of the results of attempting to group hairpins into packets and color them differentially using only the geometric packet-finding algorithm (Figure 12(a)) and a combination of this algorithm with the statistical correlation criterion for identifying strong packets and recovering their legs (Figure 12(b)). Both figures show



(a)



(b)

Figure 12. Grouping hairpins into packets using (a) the geometric packet-finding algorithm only, and (b) a combination of this algorithm and the statistical correlation criterion. Iso-surfaces of $\lambda_{ci}^2 = 4.5\lambda_{ci}^2$ are shown in white, and vortices in the same packet are highlighted with the same color.

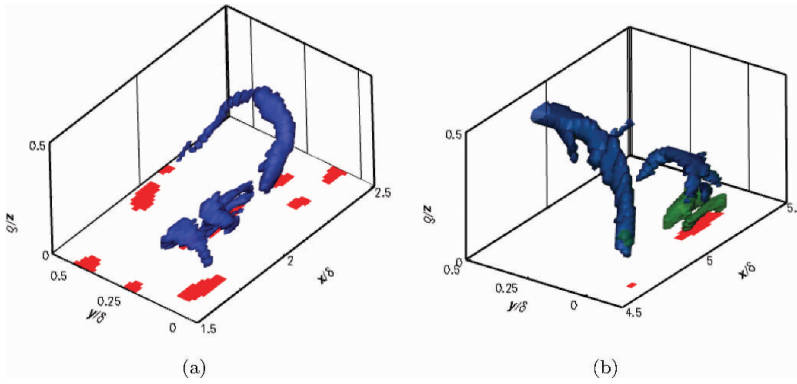


Figure 13. Reconstructed hairpin packets. The red region at the wall represents the packet's wall signature. The hairpin head vortices and their reconstructed legs are visualized using iso-surfaces of $\lambda_{ci}^2 = 4.5\lambda_{ci}^2$ shown here in blue and green respectively. (a) shows a best case scenario, where all three hairpins in the packet have been identified entirely by the packet-finding algorithm and no leg reconstruction is required. (b) shows a typical case, where one of the hairpin legs is reconstructed using the hairpin's Brown and Thomas wall signature.

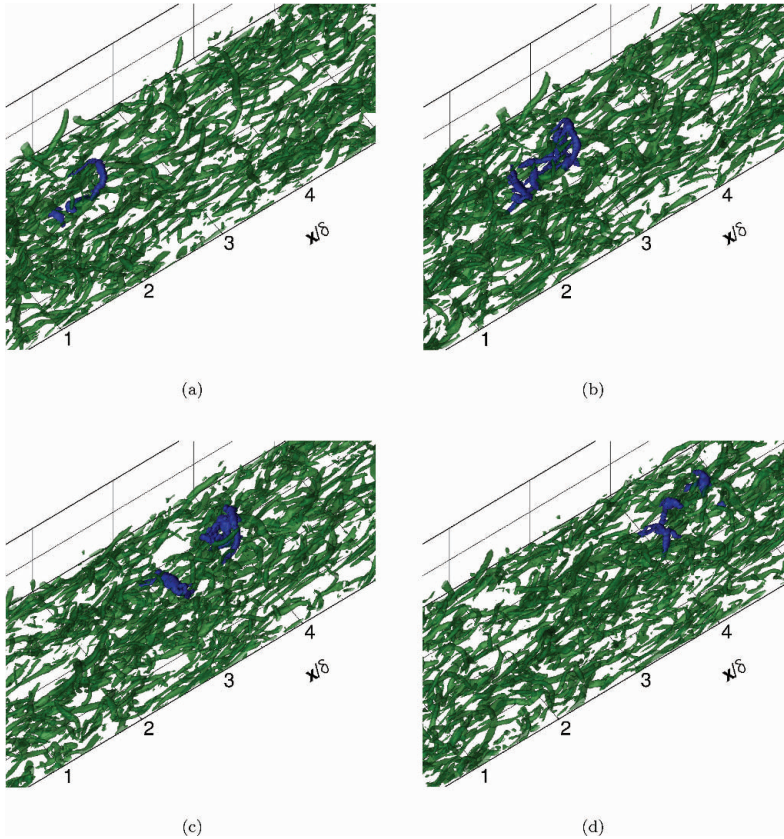


Figure 14. Tracking a hairpin packet in DNS data of a Mach 3 boundary layer at $Re_\theta = 2300$. A hairpin packet is identified in (a) and visualized using an iso-surface of swirling strength, shown here in blue. An iso-surface of swirling strength showing all other vortices is included in green and at 50% translucency. The hairpin packet was then tracked through subsequent DNS frames (b) through (d). [Click here to watch the corresponding movie.](#)

iso-surfaces of $\lambda_{ci}^2 = 4.5\bar{\lambda}_{ci}^2$ in white, and hairpins in the same packet are highlighted in the same color. Notice that in Figure 12(a) hairpins have been grouped into large packets that are not consistent with currently available evidence on the shape and size of hairpin packets. In Figure 12(b), however, several smaller strong packets have been identified. The size of the packets identified in Figure 12(b) is consistent with that reported in Ringuette et al. [2] and Adrian et al. [4].

The performance of the method for identifying and reconstructing strong packets is shown in Figure 13. In Figure 13(a) a strong packet consisting of three hairpin vortices is shown in blue. Wall signatures in the region surrounding the packet are shown in red. In this case, the hairpins in the packet were identified wholly by the geometric algorithm, so no leg reconstruction was required. Figure 13(b), on the other hand, shows a two-vortex packet where the Brown and Thomas [16] wall signatures were used to reconstruct the downstream hairpin's vortex leg (the reconstructed portions are shown in green). Figure 13(a) represents an ideal result, whereas 13(b) a typical result.

The packet in Figure 13(a) is shown again in Figure 14(a). Once again, the packet is shown in blue, but all other vortices are also included in green and at 50% translucency. This packet was then tracked through 27 DNS frames and the temporal and spatial evolution

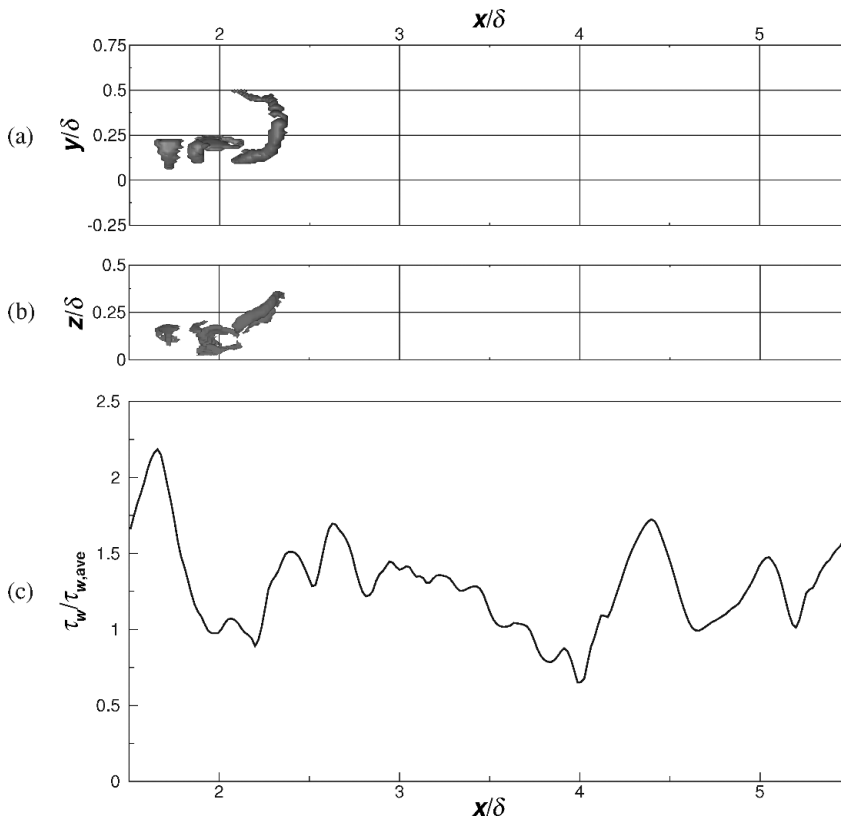


Figure 15. Evolution of the wall shear and wall pressure signals. (a) and (b) show the position of the hairpin packet using iso-surfaces of swirl strength from top and side views, respectively. (c) shows the wall shear along a streamwise line at $y/\delta = 0.25$.

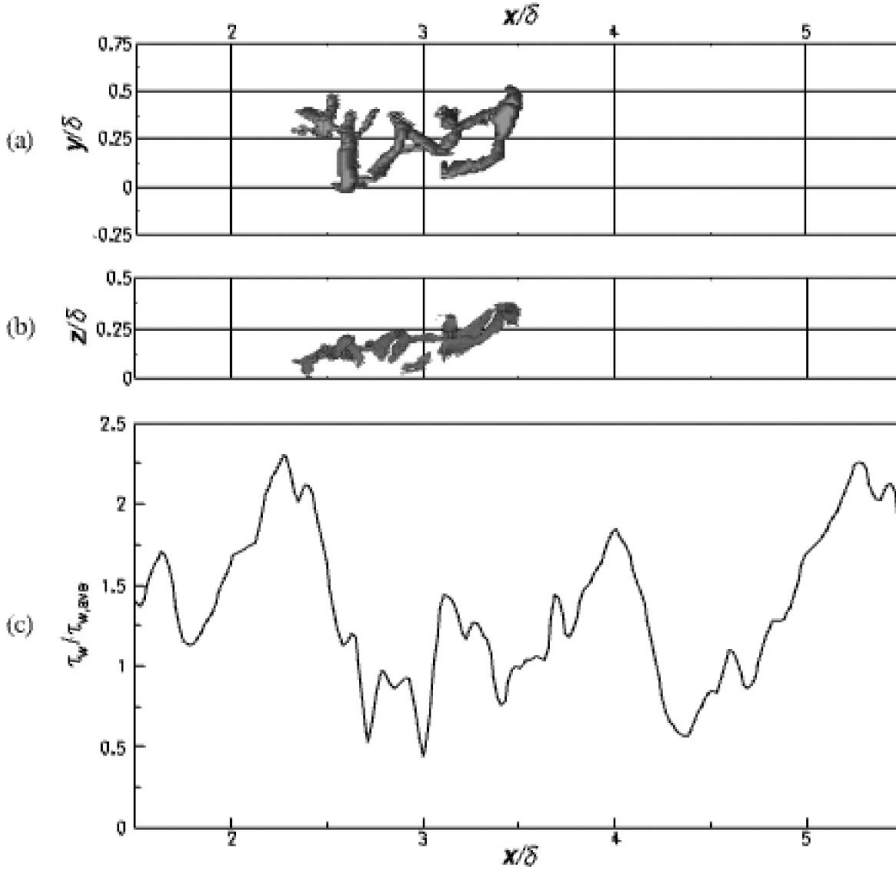


Figure 16. Evolution of the wall shear and wall pressure signals. (a) and (b) show the position of the hairpin packet using iso-surfaces of swirl strength from top and side views, respectively. (c) shows the wall shear along a streamwise line at $y/\delta_c = 0.25$. [Click here to watch the corresponding movie.](#)

of the hairpin packet was recorded into an animation included with this work. Figures 14(b) through 14(d) show the same packet at later time frames.

In addition to recording the evolution of a single packet, we also monitored the wall shear signature generated by the packet. Figures 15(a–b) show the same hairpin packet using iso-surfaces of λ_{ci}^2 from the (a) top and (b) side. Figure 15(c) shows τ_w along a line parallel to the direction of flow (the x -axis) at $y/\delta = 0.25$. The location of the line along which the wall shear was monitored corresponds to the spanwise alignment of the hairpin packet, and a peak in τ_w at approximately 1.7δ is seen to coincide with the streamwise location of the upstream end of the packet. The same quantities are plotted again in Figure 16, for a later frame. The packet has convected downstream approximately 1δ and a peak in τ_w at approximately 2.4δ is seen to again coincide with the streamwise location of the upstream end of the packet.

8. Conclusions

We use a geometric packet-finding algorithm [2] to identify hairpins and group them into packets, according to the hairpin packet model of Adrian et al. [4]. We use a correlation

analysis [16] to identify those packets with a strong wall signature and object segmentation and feature tracking algorithms [24] to track the evolution of each strong packet through multiple DNS data frames.

The swirling strength can be used by itself to identify vortical structures in a volume of data, regardless of the structure being part of a packet. The geometric algorithm using the swirl strength allows for the identification of ideal, i.e. conforming to some pre-set criteria such as those found empirically, packets in the data. The geometric algorithm together with the wall-shear and velocity correlation analysis, provide a procedure to group packets into strong, average and weak, thereby enabling conditional statistics of hairpin packets that we can isolate and visualize. It is found that packets identified using the ideal geometric criteria correspond with strong statistical packets identified using the correlation criteria, in terms of their convection velocity relative to the mean. When the tracking feature is coupled with the geometric packet identification algorithm and the wall-shear and velocity correlation analysis, the resulting tool enables autonomous tracking of individual packets to study their spatial evolution and wall signature in space and time.

Regarding the tracking procedure, the geometric algorithm by itself generally truncates hairpin legs. We find that the hairpin vortex legs can be reconstructed using the information provided by the statistical correlation analysis. Similarly, the combined object segmentation and tracking algorithm result in anti-physical proliferation of hairpinpacket structures. When we combine the physical criteria provided by the geometric algorithm and the statistical correlation analysis, we are able to isolate individual hairpin packets and successfully track them in time, automatically.

We find satisfactory results for tracking an isolated hairpin packet and the signature of the packet in time, convecting in channel flow. Similar results are obtained for a fully turbulent boundary layer at Mach 3.

The procedures for structure identification and tracking can be used in combination with experimental PIV data.

Acknowledgment

This work was supported by the National Science Foundation under CAREER Award # CTS-0238390 and a corresponding supplement by the NSF Research Experience for Undergraduates Program. Computer resources were provided by the CRoCCo Laboratory in Princeton University. We would also like to acknowledge the contributions of Professor Deborah Silver from the Department of Electrical and Computer Engineering at Rutgers University for giving us access and guidance in using the Ostrk2.0 package.

References

- [1] S.K. Robinson, *Coherent motions in turbulent boundary layers*, Annu. Rev. Fluid. Mech. 23 (1991), pp. 601–639.
- [2] M.J. Ringuette, M. Wu, and M.P. Martín, *Coherent structures in DNS of turbulent boundary layers at Mach 3*, J. Fluid Mech. 594 (2008), pp. 59–69.
- [3] B. Ganapathisubramani, E.K. Longmire, and I. Marusic, *Characteristics of vortex packets in turbulent boundary layers*, J. Fluid Mech. 478 (2003), pp. 35–46.
- [4] R. Adrian, C. Meinhart, and C. Tomkins, *Vortex organization in the outer region of the turbulent boundary layer*, J. Fluid Mech. 422 (2000), pp. 1–54.
- [5] T. Theodorsen, *Mechanism of turbulence*, 2nd. Proc. Midwestern Conf. on Fluid Mech., Columbus, OH, USA, 1952, pp. 1–19.
- [6] M. Head and P. Bandyopadhyay, *New aspects of turbulent boundary-layer structure*, J. Fluid Mech. 107 (1981), pp. 297–338.

- [7] N. Hutchins and I. Marusic, *Evidence of very long meandering features in the logarithmic region of turbulent boundary layers*, J. Fluid Mech. 579 (2007), pp. 1–28.
- [8] C.J. Delo, R.M. Kelso, and A.J. Smits, *Three-dimensional structure of a low-Reynolds-number turbulent boundary layer*, J. Fluid Mech. 512 (2004), pp. 47–83.
- [9] K.C. Kim and R.J. Adrian, *Very large scale motion in the outer layer*, Phys. Fluids. 11 (1999), pp. 417–422.
- [10] M.P. Martín, A.J. Smits, M. Wu, and M.J. Ringuette, *The turbulence structure of shockwave and boundary layer interaction in a compression corner*, AIAA paper 2006-0497 (2006).
- [11] E.M. Taylor, M.P. Martín, and A.J. Smits, *Preliminary study of the turbulence structure in supersonic boundary layers using DNS data*, AIAA Paper 2005-5290 (2005).
- [12] M.S. Chong, A.E. Perry, and B.J. Cantwell, *A general classification of three-dimensional flow fields*, Phys. Fluids. A2 (1999), pp. 765–777.
- [13] J. Zhou, R. Adrian, S. Balachandar, and T. Kendall, *Mechanisms for generating coherent packets of hairpin vortices in channel flow*, J. Fluid Mech. 387 (1999), pp. 353–396.
- [14] J. Jeong and F. Hussain, *On the identification of a vortex*, J. Fluid Mech. 285 (1995), pp. 69–94.
- [15] M.A. Green, C.W. Rowley, and G. Haller, *Detection of Lagrangian coherent structures in three-dimensional turbulence*, J. Fluid Mech. 572 (2007), pp. 111–120.
- [16] G.L. Brown and A.S.W. Thomas, *Large structure in a turbulent boundary layer*, Phys. Fluids. 10 (1977), pp. 243–251.
- [17] A.S.W. Thomas and G.L. Brown, *Large structure in a turbulent boundary layer*, in 6th Australian Hydraulics and Fluid. Mech. Conf., Adelaide, South Australia, 1977, pp. 407–410.
- [18] A.S.W. Thomas and M.K. Bull, *On the role of wall-pressure fluctuations in deterministic motions in the turbulent boundary layer*, J. Fluid Mech. 128 (1983), pp. 283–322.
- [19] B.K. Ahn, W.R. Graham, and S.A. Rizzi, *Modelling unsteady wall pressures beneath turbulent boundary layers*, AIAA paper 2004-02849 (2004).
- [20] N. Kasagi, Y. Sumitani, Y. Suzuki, and O. Iida, *Kinematics of the quasi-coherent vortical structure in near-wall turbulence*, Int. J. Heat and Fluid Flow. 16 (1995), pp. 2–10.
- [21] T.E. Burton, *Wall pressure fluctuations at smooth and rough surfaces under turbulent boundary layers with favorable and adverse pressure gradients*, MIT Report No. 70208-9, Acoustics and Vibration Lab, 1973.
- [22] W.W. Willmarth, *Structure of turbulence in boundary layers*, in *Advances in Applied Mechanics. Vol. 15*, Academic Press, Inc., New York, 1975, pp. 159–254., TVCG.
- [23] M.P. Martín, *Direct numerical simulation of hypersonic turbulent boundary layers. Part 1: Initialization and comparison with experiments*, J. Fluid Mech. 570 (2007), pp. 347–364.
- [24] X. Wang and D. Silver, *Tracking and visualizing turbulent 3D features*, IEEE TVCG. 3 (1997), pp. 129–141.
- [25] L. Jiang, *User Manual for Object-Segmentation and Feature-Tracking (ostrk2.0) Using AVS/exp Package*, Manual, Rutgers, The State University of New Jersey, 2003.